Automatic Montaging of Corneal Sub-Basal Nerve Images for the Composition of a Wide-Range Mosaic

Enea Poletti, Jeffrey Wigdahl, Pedro Guimarães, and Alfredo Ruggeri

***Abstract*—We present and discuss a computerized system able to provide a wide-range mosaic of the sub-basal nerve layer of central cornea, built from several images acquired *in-vivo* with confocal microscopy. The montage is performed by a fast, reliable and fully automatic computerized system that does not require any expedient or manual adjustment during the acquisition process. The resulting mosaic provides a large high quality image, which should significantly aid clinicians in evaluating and assessing in a more reliable way the pathologic signs of interest.**

I. Introduction

In recent years, in vivo confocal microscopy (IVCM) has grown substantially as method for a rapid and non-invasive clinical assessment of the cornea. New researches are also revealing that the subbasal nerve plexus (SNP) can be used for assessing indirectly the severity of important non-ocular conditions, such as peripheral neuropathy in diabetes or rheumatoid arthritis [1]. As new clinical implications are being discovered, more sophisticated techniques for SNP image acquisition, visualization and quantification are also being reported [2].

In recent studies, IVCM was used to elucidate the architecture of the SNP for the first time on healthy [3] and keratokonus subjects [4]. Authors manually built several mosaics from an average of 500 acquired images. Manually creating a full montage of the cornea is a hugely time-consuming process (taking from 10–20 hours depending on the number of images), because it requires a trial-and-error process of considering many hundreds of images combinations. Furthermore, some pairs of images might not be manually superimposable -only with rotations and translations- due to minor distortions related to the acquisition process.

For that reasons, computerized automation of the montage process would be very attractive to relive the incredible burden of the manual work while enabling larger scale studies to be performed. In the work presented in [5], e.g., a semi-automatic system allows the operator to minimize the manual intervention in the montaging process, and obtain a 2D mosaic image in 1.5-3 hours. A recent work [6] introduced real-time montaging of the SNP with the key benefit of a significant reduction in the time required to produce the mosaic. However, mapping quality and acquisition time were dependent on subject compliance and examiner experience. In [7], a recently reported alternative technique for using the *sequence mode* of the Rostock Corneal Module is reported. Images are captured while the subject tracks a moving target on a screen, while montaging is performed later with a custom software. This fast, semi-automated method suffers the disadvantages of reduced montage quality with fewer subbasal nerve branching details.

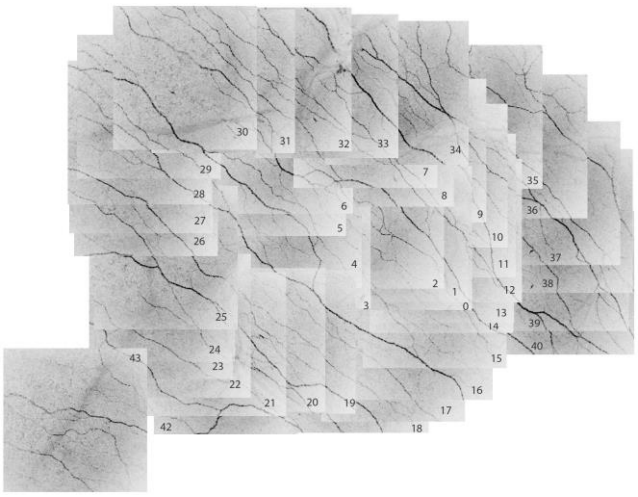

Figure 1. A manual montage of 43 images, starting from 55 acquired images. Corresponding automatic montage is shown in Fig. 3a.

The purpose of this study was to develop a system for computerized montaging of IVCM images of the corneal SNP that is fully automatic, fast, and independent on any particular expedient during acquisition.

II. Material

A laser scanning confocal microscope (IVCM; Heidelberg Retinal Tomograph 3 with Rostock Corneal Module; Heidelberg Engineering, Germany) was used in-vivo to acquire the images. Each image represented an en face view of a 400 × 400 μm corneal area. From 50 to 80 images were acquired from each eye in 4 subjects. An example of manually composed montage is shown in Fig. 1.

III. Methods

A. Outline of the algorithm

The mosaicking process is composed of 4 main steps, described below.

In order to build the final montage image, the system has to determine each image absolute position in the mosaic

Enea Poletti, JW, PG and AR are with the Department of Information Engineering, University of Padova, Padova 35131, Italy (phone: +39 049 827 7758; fax: +39 049 827 7699; e-mail: enea.poletti@dei.unipd.it).

978-1-4244-7929-0/14/$26.00 ©2014 IEEE

space. This is accomplished in the first step (sec. III-B), where an image absolute position is estimated by evaluating its position relative to the other images. In addition to the relative position, each pair of images is given a registration score, stored in the so-called registration matrix.

It might happen that the same region of the cornea is redundantly represented by several images acquired at similar (x,y), but at different z. The algorithm was equipped with a module capable of selecting, in that cluster of images, the one that contains more nerves (sec. III-C).

In the third step the actual registration between pairs of images is carried out (sec. III-D): the *N* pairs with the highest score are registered between themselves by applying translation, rotation, affinity transformations, and a custom blending procedure. After the registration of these *N* pairs, the previous steps are repeated until a final, single, large image is obtained.

For each registered pair of images, after roto-translation and affine transformation, a custom blending procedure, based on pixel intensity weighting, provides the final merged image with homogeneous luminosity and contrast and smooth transition between the two original images (sec. III-E).

B. Computation of the score matrix

The registration of two images generally involves moderate translations and rotations (due to tilting of the eye) while the need for scaling is negligible. A broad range of image registration methods have been proposed in literature [8].

The best results in our set of images were obtained with an extension of the phase correlation method, previously proposed in [9], which uses the Fourier Transforms of the two images to estimate the translation and rotation needed to register one image to the other. The method is characterized by an outstanding robustness against noise and disturbances, such as those related to non-uniform illumination. In addition, two crucial benefits of the phase correlation approach are the following: it is very fast; it automatically provides, in the process of evaluating translational and rotational data, the actual value of the correlation coefficient between the to-be registered images.

A pair of images that share a large overlap area will have a high correlation, while a low correlation will correspond to pairs of images with little or no overlap, hence impossible to register. We can then consider the phase correlation between two images as a score measuring their similarity/registrability.

The phase correlations between all pairs of images are computed and stored in the score matrix, which is symmetrical and has a unitary diagonal (hereafter, this operation will be called *hard update*). It is worth noting that at this stage the actual registration between pairs of images is not carried out yet, and that the parameter values of the phase correlation are set so as to provide a very fast and conservative evaluation of the score. This allows keeping the total running time of the procedure considerably low, despite the algorithm computational complexity of $O(N^2)$, with N the number of images.

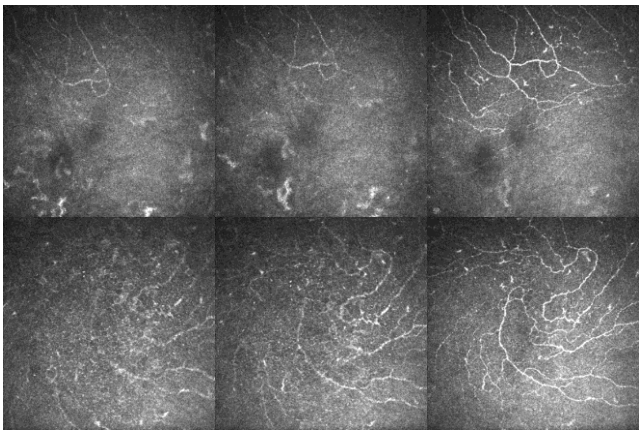

Figure 2. Two examples of clusters of three images (one in the upper row and one in the lower) highly overlapping in (x,y) but acquired at different z. The two rightmost images have been selected by the selection module because they provided the highest nerveness measure.

C. Nerveness evaluation

During the acquisition process, the operator cannot assure that the focal plan stays always constant, so the same region of the cornea (same *x*, *y*) might be acquired at different layer depths (different values of *z*). There may be sets of images that share large overlapping areas, with only some images in the set that actually contain nerves (see Fig. 2). Since this study focuses only in the subbasal nerve layer, the algorithm has been provided with a module capable of detecting the presence of nerves in an image, in order to select the most appropriate for the mosaicking composition.

For those clusters of images that share an overlapping area $> 90\%$ of their total, the algorithm evaluates the total *nerveness* of each image, and keeps only the image that shows more nerves (Fig. 2). A *nerveness* measure expresses the likelihood of an elongated structure in an image to be a nerve; in this work we employed as a *nerveness* function a formulation proposed in [10].

D. Building the Mosaic

The i^{th} column of the score matrix SM is the vector containing the scores of registration between the image i and all the other images. The sum of all the elements in the column can hence be viewed as a grade of connectivity c between the corresponding image n and all the others:

$$c_i := \sum_{n=1}^{N} SM(n,i) \qquad (1)$$

Higher values of c correspond to images that can be successfully registered with a higher number of other images, i.e., are surrounded by more overlapping images. The mosaicking algorithm starts by selecting the image with the highest c.

The mosaicking process is an iterative one: the registration is performed between the current image and the one in the score matrix that exhibits the highest value of score with the current image – let them be i and j. Only scores that

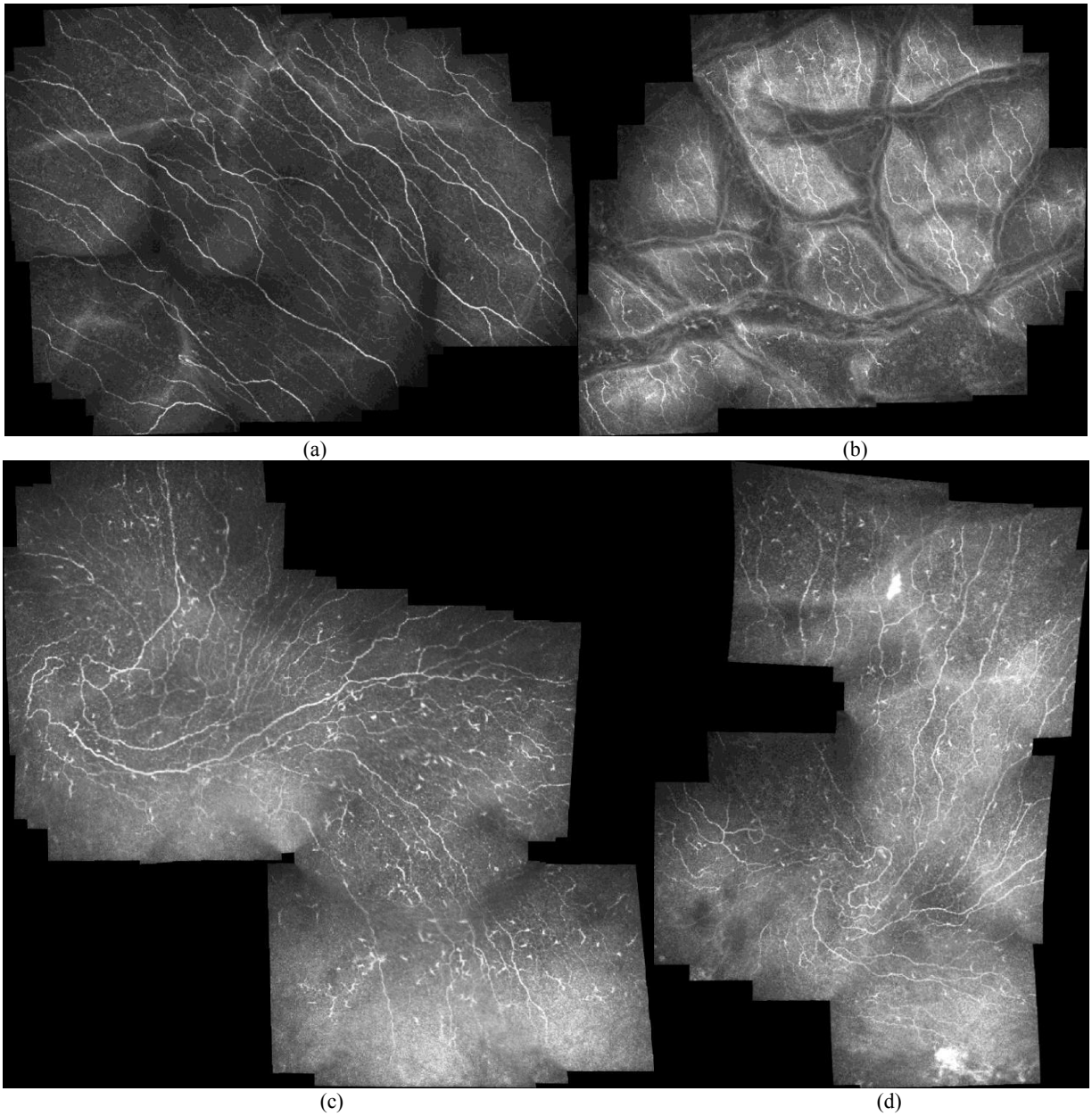

Figure 3. Four examples of obtained mosaics.

exceed an empirically set threshold are selected. The image obtained from the merging of i and j becomes the current image, and a new iteration starts until all images are merged. The process is highly efficient since it involves only $O(N)$ registrations.

Once each single registration is accomplished, the matrix score needs to be updated, since two previous images have become a single one. However, for a certain number of iterations, only a *greedy update* is carried out. For each element n of the row of i, the maximum score between i and j is kept:

$$SM(i,n) = \max[SM(i,n),\ SM(j,n)],\ \forall n \neq i \quad (2)$$

After that operation, the score column relative to j is deleted:

$$SM(j,n) = 0,\ SM(n,j) = 0\ \ \forall n \quad (3)$$

This operation can be thought as follow: for all the images not involved in the current registration, their updated correlation score with the newly composed image is equal to the best correlation score they had with one of the two composing images.

Even though the *greedy update* allows to increase time efficiency (it is $O(1)$ as opposed to $O(N^2)$ of a *hard update*), it could provide unstable results if employed for a high number of consecutive iterations (>15). This is why a *hard update* is carried out every $I = 7$ iterations, a value empirically chosen as a compromise between time efficiency and registration accuracy. It is worth noting that after each iteration the number of images to process decreases as well as the size of SM, reducing gradually the complexity of the problem.

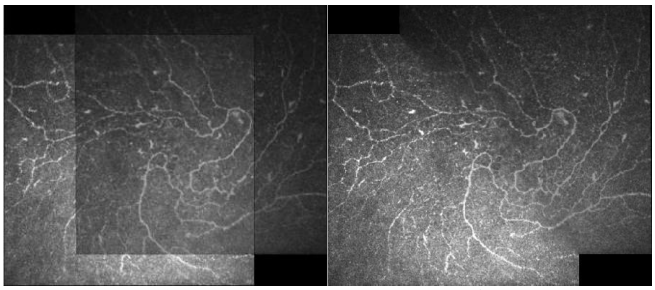

(a) (b)

Figure 4. Two example of registered images: (a) standard averaging technique; (b) with our custom blending procedure.

The single registration between two images is accomplished by using phase correlation for translation and rotation (with a different parameterization than in Sec. III-B, slower but more accurate), and affine projection for a better fine-grained matching. The parameters for the projection model are estimated by finding the correspondences between a grid of points and their matching counterpart in the overlapping area of both images.

E. Custom Blending

The registration of the images I_i and I_j will compose the new image I_{new}, which contains the region of intersection between the two original images $I_{over} := \{I_{\mathrm{i}} \cap I_{\mathrm{j2}}\} \subset I_{new}$. Since pixels in I_{over} have different values in I_i and I_j, a function f to determine these value in $I_{new}(x, y)$ is needed. A naïve method would be to assign pixel values in the overlap region would be to computing the average of the original pixels: $f(I_1, I_2, x, y) = \frac{I_1(x,y)+I_2(x,y)}{2}$ (see Fig. 4a). We designed the following weighting function:

$$f(I_1, I_2, x, y) = w_1(x, y)I_1(x, y) + w_2(x, y)I_2(x, y)$$

$$w_1(x, y) = \frac{d_1^n(x,y)}{d_1^n(x,y) + d_2^n(x,y)}, \quad w_2(x, y) = 1 - w_1(x, y) \quad (6)$$

where $d_k(x, y)$ denotes the minimum Euclidian distance between the point (x, y) and the region $I_k \backslash I_{over}$. This weighting function combines the values of pixels in the overlap region in order to obtain a smooth transition between image borders and overlap region, like as shown in Fig. 4b.

IV. RESULTS

Evaluating the performance of a mosaicking system is a difficult task. The lack of a standard methodology to compare automatic and manual montage incapacitates any attempt to compute a quantitative measure of the registration accuracy and of the montage quality.

A visual inspection of the resulting images can confirm the capability of the proposed system to provide high quality wide-range images. Fig. 3 shows four examples of final mosaic images. Mosaic areas varies from ~1000×1200μm^2 to ~1800×1600μm^2, and each is reconstructed from sets of 50 to 80 single 400×400 μm images.

Computational efficiency has been optimized in every stage of the algorithm. First score matrix computation and its successive *hard update* have a complexity of $O(N^2)$: in order to reduce their time requirement, phase correlation evaluation has been parameterized toward speed and conservativeness. Each pair of images takes ~0.08 seconds. The actual registration is accomplished by means of a second phase correlation step and affine projection. Since it involves only N images (complexity of $O(N)$), in parameterization we favored accuracy over speed. Each pair of images takes from 2.5 to 4 seconds. *Greedy update* and blending procedure are almost real time (<1 ms). The whole mosaicking operation was carried out in from 400 to 700 seconds.

As far as the nerveness evaluation module is concerned, for each mosaic an average of 5 images have been discarded. Visual inspection of each set of candidate images showed that in all cases the one with more nerves had been selected. If forcing the selection also of the discarded images, the algorithm would have provided a correctly built mosaic but with fewer visible nerves.

V. CONCLUSION

The proposed system allowed in this dataset the successful montaging of several sub-basal corneal nerve images. The resulting mosaic provides a larger, high quality image than the single original ones, which should significantly aid clinicians in evaluating and assessing in a more reliable way the pathologic signs of interest.

ACKNOWLEDGMENT

We would like to thanks Dr. Neil Lagali (Linköping University, Sweden) and Dr. Edward Lum (University of New South Wales, Australia) for having kindly provided the images used in this study.

REFERENCES

[1] Müller LJ, Marfurt CF, Kruse F, Tervo TMT. Corneal nerves: structure, contents and function. Exp Eye Res. 2003; 76: 521–542.

[2] Parissi M, Karanis G, Randjelovic S, et al. Standardized Baseline Human Corneal Subbasal Nerve Density for Clinical Investigations With Laser-Scanning in Vivo Confocal Microscopy. Investigative ophthalmology & visual science, 2013, 54.10: 7091-7102.

[3] Patel DV, McGhee CNJ. Mapping of the normal human corneal sub-basal nerve plexus by in vivo laser scanning confocal microscopy. Invest Ophthalmol Vis Sci. 2005;46:4485–4488.

[4] Patel DV, McGhee CNJ. Mapping the corneal sub-basal nerve plexus in keratoconus by in vivo laser scanning confocal microscopy. Invest Ophthalmol Vis Sci, 2005; 47(4), 1348-1351.

[5] Turuwhenua, JT, Patel, DV, McGhee, CN. Fully automated montaging of laser scanning in vivo confocal microscopy images of the human corneal subbasal nerve plexus. Invest Ophthalmol Vis Sci, 2012, 53(4), 2235-2242.

[6] Zhivov A, Blum M, Guthoff R, Stachs O. Real-time mapping of the subepithelial nerve plexus by in vivo confocal laser scanning microscopy. Br J Ophthalmol. 2010, 94:1133–1135.

[7] Efron N. The Glenn A. Fry Award Lecture 2010: Ophthalmic Markers of Diabetic Neuropathy. Optom Vis Sci. 2011; 88:661.

[8] L. Xiaoqi et al., A review of algorithm research progress for nonrigid medical image registration. Consumer Electronics, Communications and Networks (CECNet), 2011, pp.3863-3866, 16-18 April 2011.

[9] Poletti E, Benedetti G, Ruggeri A. Super-image mosaic of infant retinal fundus: Selection and registration of the best-quality frames from videos. Conf Proc IEEE Eng Med Biol Soc. 2013:5883-6.

[10] Poletti E, Ruggeri A. Automatic nerve tracking in confocal images of corneal subbasal epithelium. In: Computer-Based Medical Systems (CBMS), 2013 IEEE 26th International Symposium on. IEEE, 2013. p. 119-124.